Materials Science in Semiconductor Processing 190 (2025) 109311

Contents lists available at ScienceDirect

Materials Science in Semiconductor Processing

journal homepage: www.elsevier.com/locate/mssp

Spray-deposited EuOCl film for spectral shifters applications in silicon photovoltaic technology

Juan José Peinado Pérez [a], Francisco Martín Jiménez [b], María Cruz López Escalante [b,*]

[a] Department of Applied Physics I. Faculty of Sciences, University of Málaga, Campus de Teatinos, E-29071, Málaga, Spain
[b] Department of Chemical Engineering, Faculty of Sciences, University of Málaga, Campus de Teatinos, E-29071, Málaga, Spain

A B S T R A C T

Rare-earth oxhyhalides have great potential due to their unique 4f electronic configuration, which provides them interesting luminescent properties. Among all the possibilities, EuOCl is attracting a lot of attention because it can be stable in divalent and trivalent states providing the possibility to manage the light emission effectively. This opens up the opportunity to apply EuOCl films as spectral shifter in silicon photovoltaic technology to improve the device output power. Our study demonstrates that it is possible to prepare EuOCl films using spray pyrolysis technique and apply them as a spectral shifter to produce an relative power output improvement of 16.8 %.

1. Introduction

Today, the consideration of PV goes beyond solar farms. It will play a key role in powering electrolyzers to produce green hydrogen and achieve the total decarbonization target set by the European Union for 2050 [1–3]. In order to achieve this goal, it will be necessary to improve the efficiency of PV devices. However, the last laboratory record efficiency for c-Si cells was 6 years ago, with a value of 26.1 % in 2018 [4], very close to the theoretical value of 31 % [5]. Since then, there has been no evidence of any significant improvements in the electronic design of the cell. As a result, alternative and disruptive cell performance improvement strategies are being developed.

The use of spectral shifters is one of the most promising approaches. These are compounds derived from rare earth elements that can absorb solar radiation out of the spectral response of the solar cell and re-emit it in a wavelength range that is useful for the solar device. Depending on whether ultraviolet or infrared radiation is used, they are called down-shifters (DS) or upshifters (US). According to the bibliography, the c-Si devices can reach an efficiency of ~37 %–40 % if they are covered with ideal DS and US layers [6,7]. In addition to increasing efficiency, they can be easily implemented in all PV technologies and at cell and module level. For example, dye-sensitized solar cells (DSSC) can experiment a 30 % relative efficiency improvement by introducing Dy^{3+} doped $LaVO_4$ luminescent film on the back side [8], and organic solar cells show a 22.5 % relative improvement when a coating of Eu^{3+} doped silica-based organic-inorganic hybrid is used [9]. For silicon PV devices, the DS can be incorporated in the glass cover, by the introduction DS luminescence of Ln^{3+} ions in different host matrix with inorganic or fluoride nature (binary like CaF_2, SrF_2 and BaF_2 or ternary like $NaYF_4$ and $NaGdF_4$) [10–14]. The most notable results show relative efficiency enhancements of 20.43 % when a suitable fraction of Eu-doped phosphors mixed in a silicate film covers the monocrystalline silicon solar cell (c-Si PV solar cell) [15,16], although scaling to longer devices significantly reduces this enhancement [17].

Less explored and PV applied RE compounds are 2D REOXs (REOXs). EuOCl is an interesting compound because europium can be stable in both the bivalent and trivalent states, as Eu^{2+} and Eu^{3+}, respectively. This particularity leads to the design of materials with unique properties, as the Eu^{2+} ion exhibits emission bands ($4f^6 5\ d^1 \rightarrow 4f^7$) that can be controlled over a wide wavelength range from blue to red by tuning the local crystal symmetry and the ligand field strength due to the exposed 5d electron [18–20]. With respect to Eu^{3+} ions, they are characterized by a strong red emission via the $^5D_0 \rightarrow {}^7F_2$ transition at 616 nm together with a series of narrow photoluminescence (PL) bands in the range between 600 and 700 nm [21]. According to the bibliography, it is possible to carry out the EuOCl activation by partial substitution of Eu^{3+} with Eu^{2+}, despite the expected charge mismatch, by performing a solid-state reaction in a reducing atmosphere at 1000 °C [22]. However, the temperature preparation conditions severely limit their applications [23,24]. One of the most economical and transferable techniques for preparing films is spray pyrolysis. It has been possible to dope various oxides and sulfides with europium [25–27]. The existence of Eu^{2+} and Eu^{3+} has even been demonstrated [28].

The focus of this work is the preparation, characterization, and

* Corresponding author.
E-mail addresses: marjim@uma.es (F.M. Jiménez), mclopez@uma.es (M.C. López Escalante).

https://doi.org/10.1016/j.mssp.2025.109311
Received 24 August 2024; Received in revised form 13 January 2025; Accepted 16 January 2025
Available online 23 January 2025

application of EuOCl film on quartz substrate to be used as DS glass protective layer by spray pyrolysis. Spray pyrolysis is an economical technique that combines the ability to work at atmospheric pressure, low temperature, large area coverage and excellent industrial transfer. With the aim of increasing the adhesion, stability, and growth rate of the EuOCl film, transparent gallium oxide (Ga_2O_3) was included. The characterization has focused on the study of the structural, morphological, and chemical properties of the films. The coexistence of Eu^{2+} and Eu^{3+} has been demonstrated. Finally, by placing the samples on an industrial c-Si PV solar cell and evaluating their effect on the device output power, the films were validated as spectrally converters.

2. Experimental

2.1. Preparation of EuOCl:Ga_2O_3 film

EuOCl:Ga_2O_3 film were prepared by spray pyrolysis over commercial quartz substrate which operating is described in the bibliography [29]. The precursor solution was formed by Europium (III) Chloride Anhydrous ($EuCl_3$) in a concentration of 1.32 M in which were added 3 % molar of Gallium (III) Acetylacetonate ($Ga(AcAc)_3$). Both precursors were dissolved in 40 ml distilled water and 10 ml of acetic acid. The operational conditions were fixed at 20 ml/h flow rate and 400 °C temperature while the deposition time was varied between 2 and 35 min.

2.2. Characterization methods

The crystalline structure of the samples was examined by X-ray through a PANanalytical EMPYREAN diffractometer. Images of the morphology of the samples were obtained through field emission scanning electron microscopy (FE-SEM) using a Helios Nanolab 650 Dual Beam FEI. Elemental analysis (EDS) and high-resolution transmission electron microscope (HRTEM) images were obtained on a Talos F200X equipment. The element chemical environment was studied by X-ray photoelectron spectroscopy (XPS) using an ESCA 5701 from Physical Electronics (PHI) with monochromatic Al radiation. Optical transmittance measurements were carried out with a Varian Cary 5000 spectrophotometer with an Spectarlon sphere. Photoluminescence measurements of the samples were carried out on HORIBA Scientific photoluminescence spectrometer model Micro-PL Odyssey using 325 nm laser. The reflectance (%) of the c-Si PV solar cell was measured using a full slit with the sample holder placed in the reflectance port and the Spectralon® as the target. Absorbance was determined using the instrument software (Agilent Cary7000 UV–Vis–NIR spectrometer) and assuming zero transmission. The effect of the prepared films over the photovoltaic device have been developed by the measurement of the I-V curves in an ABA-class LED solar simulator (LSH-7320) from Oriel S.A., under standard conditions (1000 W/m^2 irradiance at 25 °C and incident spectrum AM1.5G (P_{in})), in agreement with IEC 60904-9 [30]. A commercial monocrystalline silicon solar cell manufactured by Isofoton S.A. was used for this purpose. It was a homogeneous diffusion screen-printed monocrystalline silicon solar cell with a surface area of 238.95 cm^2, a pseudo-square shape with a side length of 156 mm, an efficiency of 11.0 % and with external quantum efficiency graph presented in Figure SI1. Due to the size of the EuOCl prepared samples, the illuminated area of the solar cell was confined to a circular region of 2 cm diameter (the rest of the cell was covered with a black cardboard to keep out the radiation). The EuOCl:Ga_2O_3 samples were placed over this area and the I-V curve for each system was measured. The main I-V curve parameters under illumination conditions are short circuit current (I_{sc}), open-circuit voltage (V_{oc}), current intensity (I_{mp}), voltage at the maximum power point (V_{mp}), power at the maximum power point (P_{mp}) and fill factor (FF, Equation (1)) and efficiency (Eff, Equation (2)). With the aim to determine the influence of the EuOCl:Ga_2O_3 samples, the relative increase of P_{mp} is calculated(ΔP_{mp}, Equation (3)) The last three parameters were calculated as follows:

$$FF = \frac{P_{mp}}{I_{sc}\ V_{oc}} \bullet 100 \quad (1)$$

$$Eff = \frac{P_{mp}}{P_{in}} \bullet 100 \quad (2)$$

$$\Delta P_{mp} = \frac{P_{mp\_Eufilm} - P_{mp\_bare}}{P_{mp\_bare}} \times 100 \quad (3)$$

3. Results and discussion

3.1. Morphology characterization of the thin films

Microscopy tools have been used to characterize the deposited films. Fig. 1 shows their general morphologies where it is possible to observe how the film progressively covers the surface when the deposition time increases. Prepared sample with a deposition time of 2 min presents the typical spray droplets (Fig. 1a) which expand along the whole surface at 5 min (Fig. 1b). The superficial morphology completely changes from 7 min (Fig. 1c) where a more compact film is observed with some breakages due to the manipulation or in the case of higher deposition time due to the high deposited material quantity. In addition, the film thicknesses have been measured in each sample using transversal cross sections which are: 171 nm, 240 nm, 362 nm, 1130 nm, 1824 nm and 2570 nm for samples obtained at deposition times of 2 min, 5 min, 7 min, 12 min, 22 min and 35 min respectively. Furthermore, the punctual EDX chemical analysis developed at different points of each sample shows that samples keep stable Eu:Ga atomic ratio independently the deposition time between 2.81 and 3.32 while the Eu:Cl atomic ratio present values between 2.62 and 4.08 (average value of 3.39) for deposition time between 2 min and 7 min while it decrease until values between 1.71 and 1.89 (average value of 1.84) for deposition time between 12 min and 35 min.

3.2. Structural and chemical characterization of the thin films

Sample diffraction patterns are presented in Fig. 2 a, where it is possible to observe that only samples prepared with deposition time higher or equal than 12 min present diffraction peaks. The unique crystalline phase detected is EuOCl without any presence of other europium or gallium oxides. The diffraction pattern of EuOCl can be indexed as EuOCl phase (reference database code: 04-014-3449) according to tetragonal phase with the main diffraction peaks (101), (110) and (102) are located at angles equals of 26.089, 31.879 and 31.879 respectively.

The internal structure of one sample (12 min deposition time), has been analyzed by the characterization of a lamella at TEM microscope (Fig. 2b–j). The high-resolution TEM (HRTEM) images of the lamella (Fig. 2b) indicate that there are both crystalline and amorphous parts. In this image three regions have been marked, the first one with purple circle, the second one with blue circle and the last one with arrows which are related with EuOCl, Ga_2O_3 and amorphous domains. In addition, the interplanar spacing of the two crystalline regions have been determined indicating values of 3.43 Å assigned to the (101) plane for EuOCl compound and 2.66 Å assigned to the (104) plane for Ga_2O_3. Concerning the chemical images (Fig. 2c–i), they show a dense structure neither the presence of pinholes nor inclusions just small irregularities are detected at the surface which can be more related with the thin film manipulation instead of the preparation method. In addition, the chemical analysis of the lamella has been carried out. The registered chemical maps show that the main elements, Eu, Cl, Ga and O, are distributed along the whole lamella where no diffusion neither Si (quartz substrate) nor Pt (sample manipulation to obtain the lamella) are detected. It is interesting to point out the Ga behavior where a

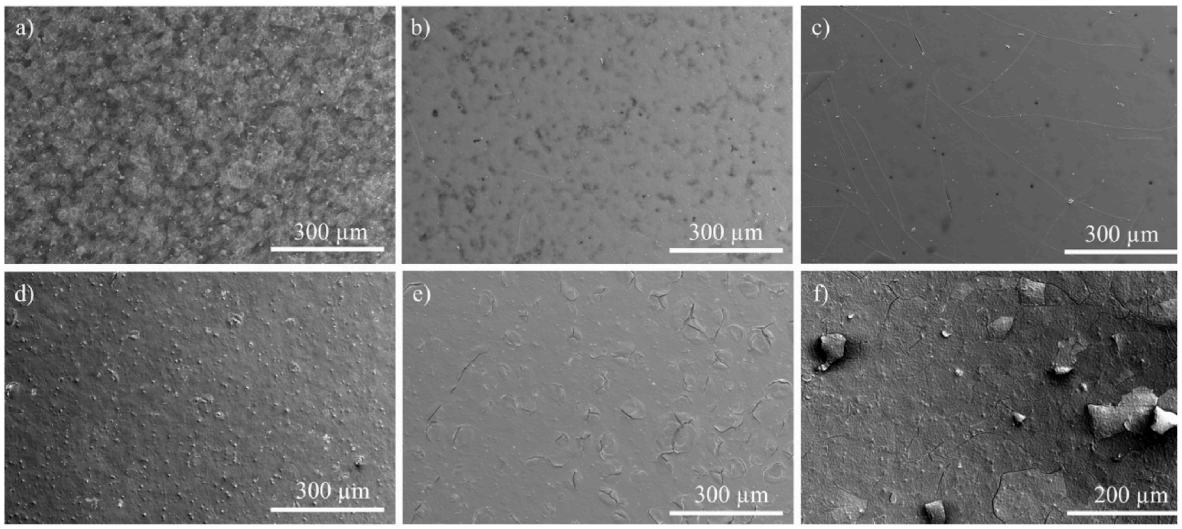

Fig. 1. Morphological study of the surface sample obtained at different deposition times: a) 2 min, b) 5 min, c) 7 min, d) 12 min, e) 22 min, f) 35 min.

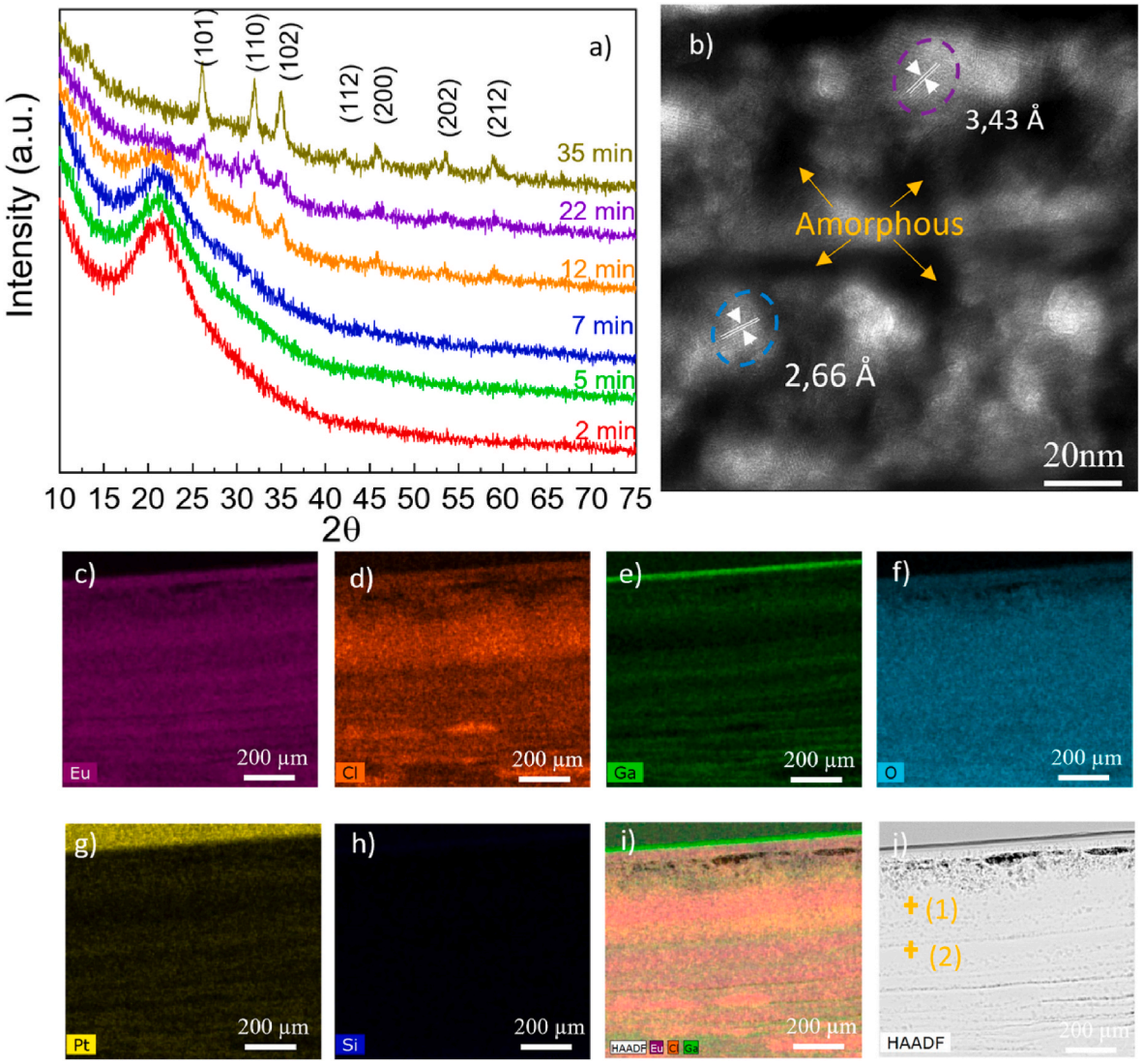

Fig. 2. Structural analysis of the samples: a) XRD pattern or EuOCl:Ga_2O_3 thin films with different deposition times, b) HRTEM image of EuOCl:Ga_2O_3 thin film with deposition time of 12 min, c-i) EDX elemental mapping, j) HAADF image.

preferential laminar distribution driven to a quasy-horizontal lines leading to great differences in composition. This effect has been quantified by developing the chemical analysis of two different points (Fig. 2h) with extreme concentrations. The first one with a higher Eu concentration (named as 1) and the second one with a higher Ga concentration (named as 2) where the Eu:Ga atomic values are 81:19 (ratio 4.2) and 54:46 (ratio 1.2) respectively. The rest of points present values in between.

The oxidation state analysis together with the environment influence have been analyzed by XPS for all the samples at raw surface and after a soft Ar^{+} bombardment of 1 min. As can be observed in Fig. 3a, the bombardment does not perform any negative nor significative effect over the surface and just allows to obtain more defined signals. This Fig. allows to appreciate the clear presence of two of the main elements involved in the thin film composition, this is Ga and Eu. The Ga 2p and Eu 3d core level regions for all the prepared samples are showed in Fig. 3b. The registered peaks are related with Ga^{3+}, Eu^{3+} and Eu^{2+} chemical species which bands have been assigned as follows: the first pair located at 1117.86 and 1144.78 are related with Ga $2p_{3/2}$ and Ga $2p_{1/2}$ in the form of Ga_2O_3 the second pair centered at 1125.07 eV and 1155.19 eV are assigned to Eu^{2+} $3d_{5/2}$ and Eu^{2+} $3d_{3/2}$ and the last couple detected at 1134.68 eV 1164.32 eV is attributed to Eu^{3+} $3d_{5/2}$ and Eu^{3+} $3d_{3/2}$ respectively [31], confirming the presence of both, Eu^{2+} (3d4f [7]) and Eu^{3+} (3d4f [6]) [32]. A detailed comparison between the species reveals that independently of the sample two tendencies are presented: the first one is that the Eu^{3+} contribution is always much higher than Eu^{2+}contribution and the second one is that the Ga^{3+} $2p_{3/2}$ peak intensity grows up with the increment of deposition time when it is compared with Eu^{3+} $3d_{5/2}$ signal. This last effect can be related with the previously observed segregation material process inside the sample because the more deposition time is implemented the more Ga_2O_3 linear regions can be placed at the surface and taking in mind that XPS is a surface analytic tool, the element segregation effect is determinant. Fig. 3 c and d present the O 1s and Cl 2p spectra for all the samples with considerable intensity. Additionally, it is possible to determine the Eu^{2+}@Eu^{3+} atomic distribution by XPS fitted areas which are: 8.48@91.51, 6.13@93.86, 8.71@91.29, 10.68@89.32, 11.60@88.40 and 8.80@91.20 for 2 min, 5 min, 7 min, 12 min, 22 min and 35 min

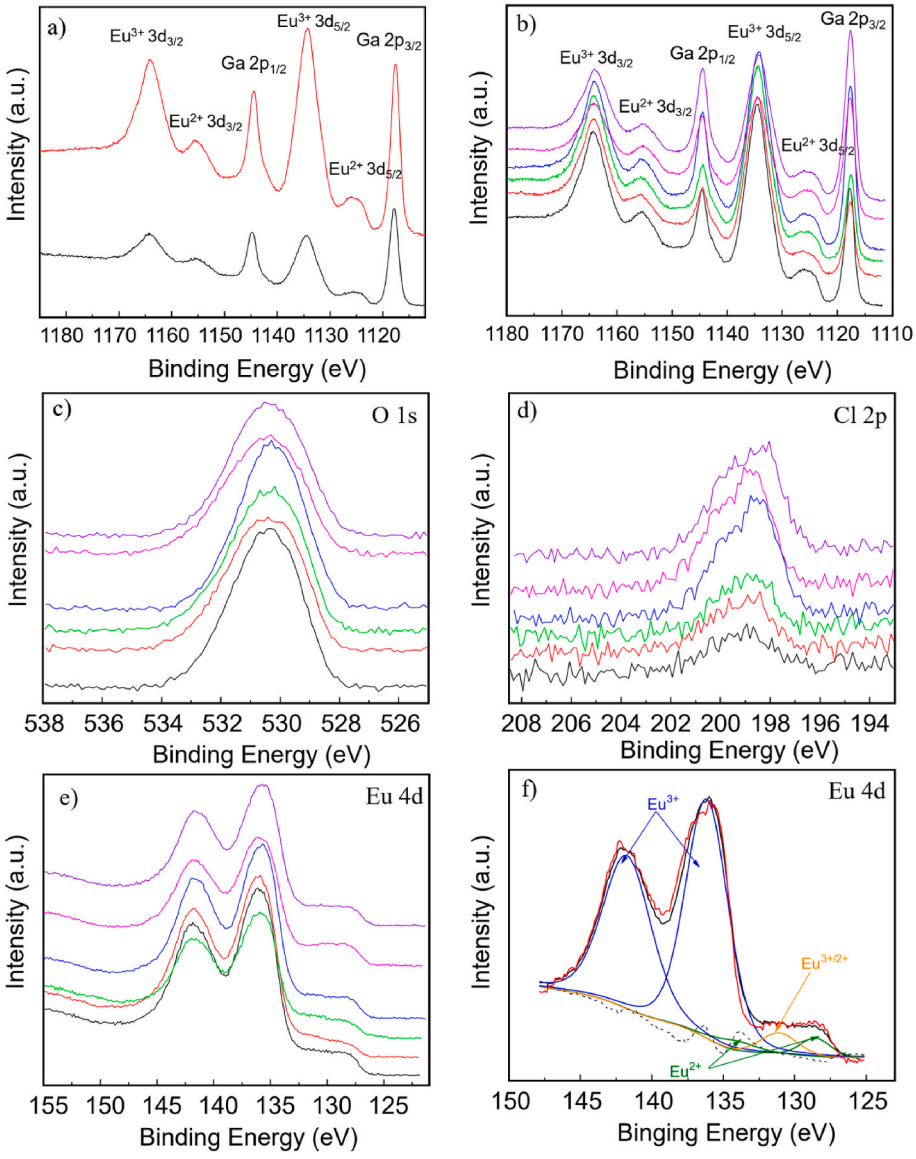

Fig. 3. XPS spectra of EuOCl:Ga_2O_3 thin film with deposition time of 12 min, a) Eu 3d and Ga 2p region for raw (black) and after sputtering (red); b) Eu 3d and Ga 2p core level spectra; c) O 1s core level spectra; d) Cl 2p core level spectra; e) Eu 4d core level spectra for different deposition times: 2 min (black), 5 min (red), 7 min (green), 12 min (blue), 22 min (magenta), 35 min (purple); f) Eu 4d core level deconvolution for 12 min of deposition time. (For interpretation of the references to colour in this figure legend, the reader is referred to the Web version of this article.)

deposition time respectively. These values indicate that self-reduction procedure is performed with higher efficiency at those samples prepared at 12 min and 22 min. Fig. 3e, presents the Eu 4d core level for all the samples where the same three different main contributions can be identified. Fig. 3f depicts the Eu 4d core level deconvolution for 12 min time deposition sample where the three peaks have been adjusted: the first pair is located at 135.98 eV and 141.58 eV are assigned at Eu^{3+} $4d_{5/2}$ and Eu^{3+} $4d_{3/2}$ respectively (blue peaks) and it is related with the EuOCl red-emission; the second pair is located at 128.44 eV and 134.04 eV correspond to Eu^{2+} $4d_{5/2}$ and Eu^{2+} $4d_{3/2}$ respectively (green peaks) with the spin-orbital splitting values for the Eu^{3+} and Eu^{2+} species is 5.6 eV and finally a middle band at 130.65 eV assigned to a mixed valence state, Eu^{3+}/Eu^{2+} (orange peak) and related with the blue emitting EuOCl compounds response [22,33]. This deconvolution allows to determine the percentage $(Eu^{3+}/Eu^{2+})/Eu^{3+}$ per sample which are: 8.1 %, 9.0 %, 13.3 %, 13.1 %, 10.0 % and 7.6 % 2 min, 5 min, 7 min, 12 min, 22 min and 35 min deposition time respectively.

3.3. Optical and photoluminescence properties of the thin films

The optical properties of the whole prepared sample set are presented in Fig. 4. Regarding the transmittance spectra (Fig. 4a) it is possible to observe that they present real flat spectra with transmittance between 89 % and 87 % at a wavelength of 700 nm for samples with deposition time between 2 min and 12 min. The transmittance value for samples prepared with higher deposition time are lower to 80 % due to the high quantity of deposited material which leads to thicker films. At lower wavelength it is noticeable a shoulder located around 260 nm which can be related with the radiation absorption process developed by the film. This wavelength range can be related to the absorption of the matrix corresponding to the transition from the valence band to the conduction band but could also overlap the transition associated with the O–Eu charge transfer band [34]. The optical band gap of the samples has been calculated and samples between 2 min and 12 min are quite similar with 4.40 eV as average value (between 4.53 eV and 4.10 eV) which is near to the reference value of 4.60 eV (Fig. 4b) with the most massive samples present a drastically reduction until 3.81 eV related with the high thickness of both samples [22].

The emission spectra of the prepared samples are presented in Fig. 5. The strongest red emission peak is located at 613 nm which is assigned to $^5D_0 \rightarrow {}^7F_2$ transition for Eu^{3+} (Fig. 5a). This signal is presented in the six prepared samples independently of the deposition time [35–37]. In addition, other photoemission peaks are exhibited at 578, 587, 651 and 702 nm which can be related to $^5D_0 \rightarrow {}^7F_0$, $^5D_0 \rightarrow {}^7F_1$, $^5D_0 \rightarrow {}^7F_3$ and $^5D_0 \rightarrow {}^7F_4$ transitions, respectively and they are assigned to Eu^{3+} specie and linked with its red emission. As it is expected, the position of the peaks does not change with deposition time the position of the peaks does not change with deposition time. In addition, when a closer view is carried out by of the graph a zoom of the ultraviolet-blue region (Fig. 5 b), two broad band emission with maximums at 406 nm and 487 nm are detected. They can be related with $4f^6 5\,d^1 \rightarrow 4f^7$ transition for Eu^{2+} and $Eu^{2+/3+}$ respectively [6,23]. In accordance with the emission spectra of the as-prepared samples a proposed assignment of the emission and absorption transitions is shown in Fig. 5c. With the measurements performed so far, transmission, absorption and PL, it is not possible to determine which is the optimal layer thickness that can influence the photovoltaic performance of the solar cell. Therefore, it is necessary to measure the I-V curves [6,38,39].

3.4. I-V measurements

This section is dedicated to the evaluation of the performance variations caused by the prepared samples when deposited on a commercial silicon solar cell. Before developing the I-V curve measurement, it is convenient to integrate the PL spectra (12 and 35 min of deposition time) with the absorption spectrum of a silicon solar cell (Fig. 6a) and the cut-off wavelength of the encapsulant (orange line) [35]. From Fig. 6a, it can be seen that the response of a silicon solar cell is in the range between 350 nm and 1100 nm. However, its maximum absorbance is reduced to a narrower range between 500 nm and 800 nm. The PL spectrum of the EuOCl layers is completely in the former range, remaining away from the upper wavelength cut-off of the polymer [40].

Taking this in mind and with the aim to measure the effect over real standard silicon PV cell, the prepared samples and a substrate have been placed on top of the solar device and the I-V curve have been measured under standard conditions. Results are presented in Fig. 6b and the obtained numerical values are summarized in Table 1 I-V curves first sight show a significative I_{sc} parameter variation with respect the reference while V_{oc} parameter keeps similar in all the measurements which implies that P_{mp} variations are mainly due to current differences which in turn is directly related to the radiation management. The reading of Table 1 indicates that the current parameter improvement, I_{sc} and/or I_{mp}, comes from samples with thin films with deposition times between 5 min and 12 min, where the power increase from reference value of 50.78 mW (10.36 % in efficiency) to 59.30 mW (12.10 % in efficiency) which implies a P_{mp} relative difference (ΔP_{mp}) of 16.8 %, calculated according to equation (3) (1.74 % efficiency increment). The I-V curve measurements from 22 min to 35 min deposited time samples reduce the P_{mp} parameter until 37.7 mW, this is a relative difference of −25.8 % (−2.67 % in efficiency) directly related with the fact that the

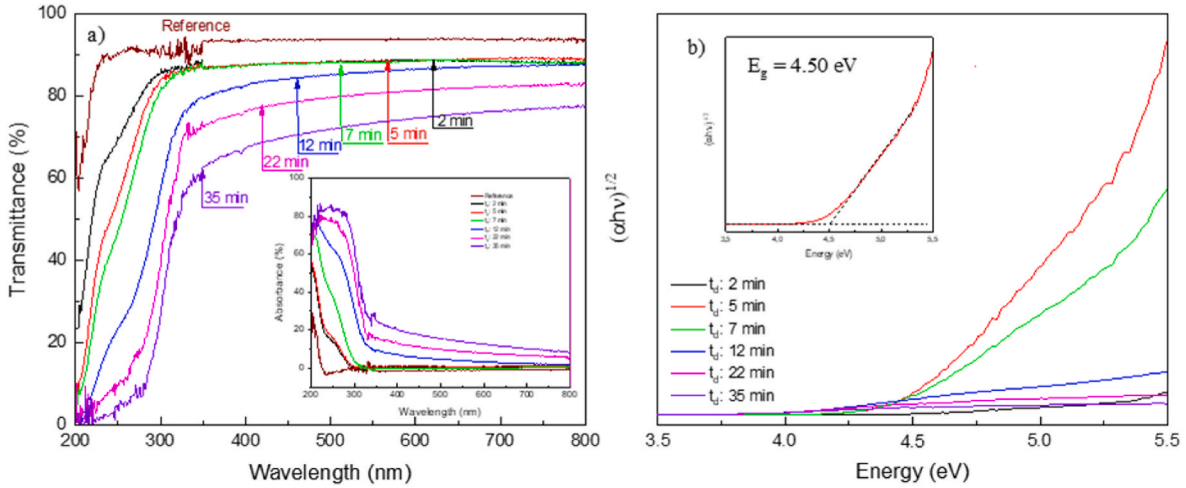

Fig. 4. Optical properties of $EuOCl:Ga_2O_3$ thin film with different deposition times: a) transmission and absorption spectra (inset) and b) band gap determination.

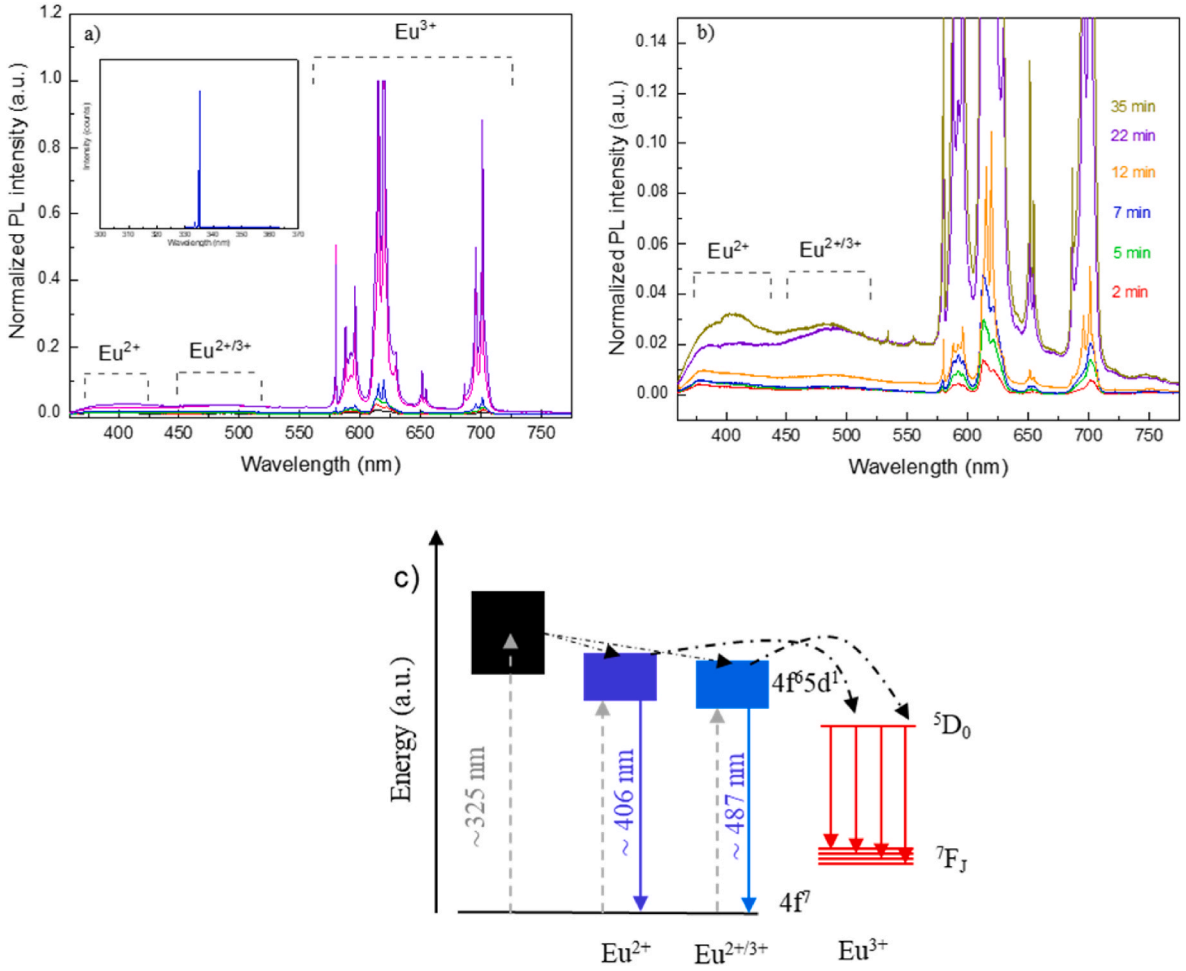

Fig. 5. Photoluminescence response of the samples: a) EuOCl:Ga_2O_3 thin film for different deposition times: 2 min (black), 5 min (red), 7 min (green), 12 min (blue), 22 min (magenta), 35 min (purple) and the excitation spectra of the laser (inset); b) a magnification of the photoluminescence; c) proposed photoluminescence mechanism of the Eu species. (For interpretation of the references to colour in this figure legend, the reader is referred to the Web version of this article.)

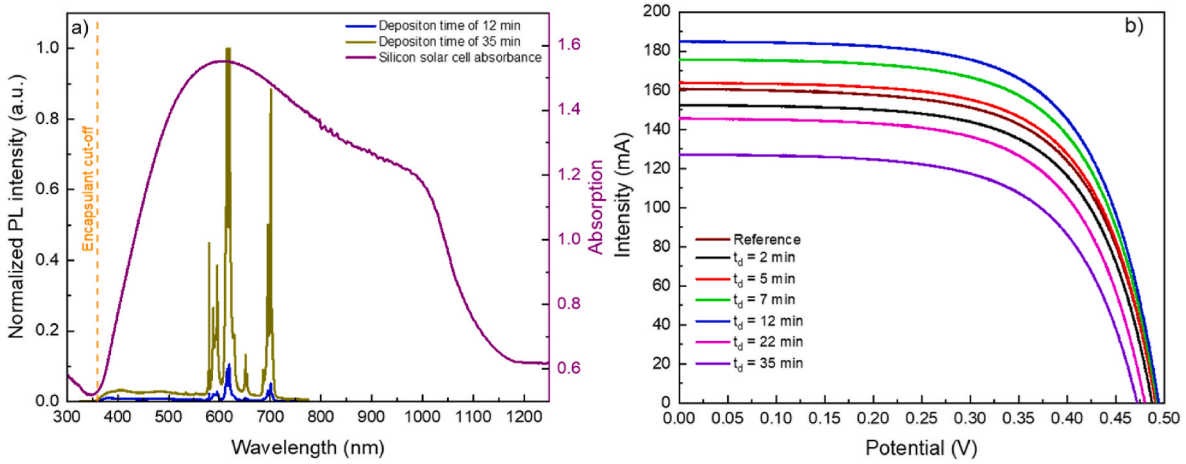

Fig. 6. Photovoltaic response of the samples: a) Photoluminescence response of the samples: EuOCl:Ga_2O_3 thin film for 12 and 35 min of deposition times together with the absorbance spectrum of a commercial silicon solar cell:; b) I-V curve measurement. (For interpretation of the references to colour in this figure legend, the reader is referred to the Web version of this article.)

radiation does not reach the silicon surface due to the thick film thickness. In terms of measurement uncertainty, the maximum variation measured in power is ± 0.004 % is less than ± 2 %, corresponding to an ABA solar simulator.

4. Conclusions

In conclusion, EuOCl thin films of different thicknesses have been successfully prepared by chemical spray pyrolysis using an interlaminar

Table 1
Measured parameters of the I-V curve parameters for the different EuOCl:Ga_2O_3 samples placed on top of the c-Si PV solar cell.

Time (min)	I_{sc} (mA)	V_{oc} (mV)	P_{mp} (mW)	FF (%)	Eff (%)	ΔP_{mp} (%)	Diff. Eff (%)
0	160	491	50.8	64.64	10.36		
2	152	487	47.9	64.71	9.78	−5.7	−0.58
5	164	490	52.1	64.83	10.63	+2.6	+0.27
7	176	490	56.1	65.05	11.45	+10.5	+1.09
12	185	490	59.3	65.42	12.10	+16.8	+1.74
22	147	480	44.6	63.21	9.10	−12.2	−1.26
35	127	470	37.7	63.16	7.69	−25.8	−2.67

Ga_2O_3 film for mechanical stability. Micrographs show that the films cover the substrate surface homogeneously. They show a natural segregation of Ga_2O_3 forming quasilinear films inside the sample. In addition, structural and chemical analyses show that the sample is crystalline after 12 min. It has a high $Eu^{3+}/Eu^{2+})/Eu^{3+}$, 13.1 %, and the Eu:Cl atomic ratio goes from average values of 3.39 to 1.84. Finally, the XPS study reveals the presence of Ga_2O_3 and EuOCl. The self-reduction process of Europium leads to the formation of Eu^{2+} from Eu^{3+}. In terms of optical properties, samples with a deposition time of less than 12 min show a transmittance at 700 nm between 89 % and 87 %. This transmittance decreases to 80 % for longer deposition times. Regarding photoemission, all samples show the $^5D_0 \rightarrow {}^7F_2$ transition for Eu^{3+} with strong localized emission at 613 nm, accompanied by the remaining signals related to this species. In addition, samples with a deposition time longer than 12 min show a broad band in the ultraviolet-blue region located at 406 nm and 487 nm. These bands are assigned to the $4f^6 5\,d^1 \rightarrow 4f^7$ transition for Eu^{2+} and $Eu^{2+/3+}$respectively.

Finally, the measured I-V curves of the solar cell, without and with the EuOCl films deposited, show that there is an increase in power for samples with deposition times between 5 and 12 min. A maximum relative difference of 16.8 % is observed. However, the high thickness of the samples prepared with longer deposition times leads to a significant absorption of radiation and consequently to a reduction in power.

CRediT authorship contribution statement

Juan José Peinado Pérez: Data curation. **Francisco Martín Jiménez:** Writing – review & editing, Funding acquisition. **María Cruz López Escalante:** Writing – review & editing, Writing – original draft, Visualization, Methodology, Investigation, Formal analysis, Data curation, Conceptualization.

Declaration of competing interest

The authors declare that they have no known competing financial interests or personal relationships that could have appeared to influence the work reported in this paper.

Acknowledgements

This research was financed by project PID2020–117832RB-100 MCIN/AEI/10.13039/501100011033, Spain and FQM192-G-FEDER 2023-2025 (PEC Y PV-PEC para la fotoelectrolisis solar del agua)

Appendix A. Supplementary data

Supplementary data to this article can be found online at https://doi.org/10.1016/j.mssp.2025.109311.

Data availability

Data will be made available on request.

References

[1] Estrategia a largo plazo para una economía española moderna, competitiva y climáticamente neutra en 2050. Ministerio para la Transición Ecológica y el Reto Demográfico (chrome-extension://efaidnbmnnnibpcajpcglclefindmkaj/https://ec.europa.eu/clima/sites/lts/lts_es_es.pdf) (last access: 2024/12/09).
[2] Hoja de ruta del hidrógeno: una apuesta por el hidrógeno renovable. Ministerio de Transición & Reto Demográfico (chrome-extension://efaidnbmnnnibpcajpcglclefindmkaj/https://www.miteco.gob.es/content/dam/miteco/es/ministerio/planes-estrategias/hidrogeno/hojarutahidrogenorenovable_tcm30-525000.PDF (last access: 2024/12/09).
[3] Plan Nacional integrado de energía y clima 2021-2030. Ministerio para la Transición Ecológica y el Reto Demográfico (chrome-extension://efaidnbmnnnibpcajpcglclefindmkaj/https://www.miteco.gob.es/content/dam/miteco/images/es/pnieccompleto_tcm30-508410.pdf)) (last access: 2024/12/09).
[4] Best Research- Cell Efficiency Chart (https://www.nrel.gov/pv/cell-efficiency.html) (last access: 2024/12/09).
[5] W. Shockley, H.J. Queisser, Detailed balance limit of efficiency of p-n junction solar cells, J. Appl. Phys. 32 (2004) 510–519.
[6] A. Boccolini, J. Marques-Hueso, D. Chen, Y. Wang, B.S. Richards, Physical Performance Limitations of Luminescent Down-Conversion Layers for Photovoltaic Applications, 2013, https://doi.org/10.1016/j.solmat.2013.11.005.
[7] A.R. Zanatta, The Shockley–Queisser limit and the conversion efficiency of silicon-based solar cells, Res. Opt. 9 (2022).
[8] J. Liu, Q. Yao, Y. Li, Effects of downconversion luminescent film in dye-sensitized solar cells, Appl. Phys. Lett. 88 (2006).
[9] J. Farinhas, et al., Ultraviolet-filtering luminescent transparent coatings for high-performance PTB7-Th:ITIC–Based organic solar cells, Front. Nanotechnol. 3 (2021).
[10] R.K. Sharma, et al., Eu-doped BaF_2 nanoparticles for bioimaging applications, ACS Appl. Nano Mater. 2 (2019) 927–936.
[11] V. Kale, M. Lastusaari, J. Hölsä, T. Soukka, Intense UV upconversion through highly sensitized $NaRF_4$:Tm (R:Y,Yb) crystals, RSC Adv. 5 (2015) 35858–35865.
[12] X. Zhang, et al., Magnetic and optical properties of $NaGdF_4$:Nd^{3+}, Yb^{3+}, Tm^{3+} nanocrystals with upconversion/downconversion luminescence from visible to the near-infrared second window, Nano Res. 8 (2015) 636–648.
[13] S. Balabhadra, M.F. Reid, V. Golovko, J.P.R. Wells, Absorption spectra, defect site distribution and upconversion excitation spectra of $CaF_2/SrF_2/BaF_2$:Yb^{3+}:Er^{3+} nanoparticles, J. Alloys Compd. 834 (2020).
[14] T. Samanta, S.K. Jana, A.E. Praveen, V. Mahalingam, Ligand sensitized strong luminescence from Eu^{3+}-doped $LiYF_4$ nanocrystals: a photon down-shifting strategy to increase solar-to-current conversion efficiency, Dalton Trans. 46 (2017) 9646–9653.
[15] W.J. Ho, et al., Photovoltaic performance enhancement of silicon solar cells based on combined ratios of three species of europium-doped phosphors, Materials 11 (2018).
[16] W.J. Ho, Y.T. Shen, J.J. Liu, B.J. You, C.H. Ho, Enhancing photovoltaic performance using broadband luminescent down-shifting by combining multiple species of Eu-doped silicate phosphors, Nanomaterials 7 (2017).
[17] J. Liu, et al., Improving spectral response of monocrystalline silicon photovoltaic modules using high efficient luminescent down-shifting Eu^{3+} complexes, Prog. Photovoltaics Res. Appl. 21 (2013) 668–675.
[18] J. Li, et al., Highly efficient and air-stable Eu(II)-containing azacryptates ready for organic light-emitting diodes, Nat. Commun. 11 (2020) 1–8, 2020 11:1.
[19] S. Ding, H. Li, J. Li, Y. Wang, Abnormal self-reduction phenomenon of europium-doped borate and its luminescence properties, ACS Appl. Electron. Mater. 3 (2021) 2774–2782.
[20] L. Yang, et al., Tunable color emitting of $Ba_{1-x-y}SiO_{3:x}Eu,yBi^{3+}$ phosphors with the self-reduction of Eu^{3+} ions calcined in air, J. Lumin. 203 (2018) 500–506.
[21] Z. Yang, L. Yang, Y. Pu, D. Chuan Zhu, The effect and mechanism of different charge compensation on the luminescent properties of Eu-doped $BaSiO_3$ phosphor calcined in air with self-reduction, Opt. Mater. 114 (2021) 110981.
[22] D. Kim, et al., Self-emitting blue and red EuO_X (X = F, Cl, Br, I) materials: band structure, charge transfer energy, and emission energy, Phys. Chem. Chem. Phys. 21 (2019) 1737–1749.
[23] Y. Bai, et al., Excitons in strain-induced one-dimensional moiré potentials at transition metal dichalcogenide heterojunctions, Nat. Mater. 19 (2020) 1068–1073, 2020 19:10.
[24] P. Chen, et al., Recent Advances in 2D Rare Earth Materials, 2020, https://doi.org/10.1002/adfm.202008790.
[25] A.M.S. Arulanantham, et al., Photosensitivity properties of Eu-doped SnS_2 thin films deposited by cost-effective nebulizer spray pyrolysis technique, Appl. Phys. A 128 (2022) 364.
[26] S.W. Li, et al., Synthesis and characterization of Eu^{3+} doped TiO_2 thin films deposited by spray pyrolysis technique for photocatalytic application, Mater. Res. Express 8 (2021) 026402.
[27] M.D. Devi, et al., Enhancement in Optoelectronic Properties of Europium-Doped ZnS Thin Films Prepared by Nebulizer Spray Technique for UV Photodetection Applications, 2022, https://doi.org/10.1016/j.mssp.2022.106572.
[28] A. Nebatti Ech-Chergui, et al., Spray pyrolysis-assisted fabrication of Eu-doped ZnO thin films for antibacterial activities under visible light irradiation, Chem. Pap. 77 (2023) 1047–1058.
[29] R. Romero, et al., Silver zirconium oxide cermet coatings spray deposited onto galvanized steel sheet for low temperature solar applications, Ceram. Int. 49 (2023) 33643–33651.

[30] UNE-EN IEC 60904-9:2021, Photovoltaic Devices–Part 9: Classification of Solar Simulator Characteristics, International Standard, Geneve, Swizerland, 2021.
[31] J.F. Moulder, W. F. S. P. E. S. K. D. B. Handbook of X-Ray Photoelectron Spectroscopy. *Published by* Physical Electronics, Inc.
[32] B. Park, et al., Tunable wide blue photoluminescence with europium decorated graphene, This journal is Cite this: J. Mater. Chem. C 4030 (2015) 4030.
[33] Y. Ro, S. Park, Y.J. Cho, D.H. Kim, Enhanced activity and selectivity of supported europium oxychloride catalysts for ethylene oxychlorination with HCl, Mol. Catal. 516 (2021).
[34] H. Kamioka, M. Hirano, H. Hosono, Photo-induced charge state conversion of Eu^{2+} in Ca2 ZnSi2 O7, J. Appl. Phys. 106 (2009) 53105.
[35] Z. Chen, et al., The impact of dopant contents on structures, morphologies and optical properties of Eu doped Ga_2O_3 films on GaAs substrate, J. Lumin. 194 (2018) 374–378.
[36] A. Layek, et al., Dual europium luminescence centers in colloidal Ga_2O_3 nanocrystals: controlled in situ reduction of Eu(III) and stabilization of Eu(II), Chem. Mater. 27 (2015) 6030–6037.
[37] A.A. Nashivochnikov, et al., Shaping the photoluminescence spectrum of ZrO_2:Eu^{3+} phosphor in dependence on the Eu concentration, Opt. Mater. 121 (2021) 111620.
[38] A. Boccolini, J. Marques-Hueso, B.S. Richards, Self-absorption in upconverter luminescent layers: impact on quantum yield measurements and on designing optimized photovoltaic devices, Opt. Lett. 39 (2014) 2904.
[39] R.M. Gunji, G.R.S. Mattos, C.D.S. Bordon, L.A. Gó-Malaga On, L.R.P. Kassab, Efficiency enhancement of silicon solar cells covered by GeO_2-PbO glasses doped with Eu^{3+} and TiO_2 nanoparticles, J. Lumin. 223 (2020) 117244.
[40] M.C. López-Escalante, L.J. Caballero, F. Martín, M. Gabás, J.R. Ramos-Barrado, Selective emitter technology global implantation through the use of low ultraviolet cut-off EVA, Sol. Energy Mater. Sol. Cell. 159 (2017) 467–474.